Ordering fluctuation dynamics in AuAgZn 2

Frédéric Livet, Mathieu Fèvre, Guillaume Beutier, Mark Sutton

Ordering fluctuation dynamics in AuAgZn$_2$

Frédéric Livet[1,2*], Mathieu Fèvre[3], Guillaume Beutier[1,2], and Mark Sutton[4]

[1] *Univ. Grenoble Alpes, SIMAP, F-38000 Grenoble, France*
[2] *CNRS, SIMAP, F-38000 Grenoble, France*
[3] *Laboratoire d'Etude des Microstructures, UMR 104 CNRS-ONERA, BP 72, 92322 Châtillon, France and*
[4] *Center of the Physics of Materials, McGill University,*
3600 University street, Montreal, PQ, Canada, H3A-2T8

(Dated: August 18, 2015)

The second-order ordering transition of the AuAgZn$_2$ alloy has been studied by coherent x-ray scattering. Within a few degrees above the critical temperature T_c, equilibrium critical fluctuations are observed together with some pre-transitional local ordering connected to sample defects. The speckles observed correspond to heterodyne interference between local ordering and fluctuations and show a mixed static and dynamical behaviour in a narrow domain of a few tenths of degree above T_c. The dynamical behaviour is shown to correspond to the critical slowing down of the fluctuations in the vicinity of the transition (model "A" of Hohenberg and Halperin[1]). A rough comparison can be carried out with the classical diffusion models. Some improvements of the method are discussed.

I. INTRODUCTION

When a system is close to the critical point, anomalies occur in its static properties, like the divergence of the fluctuation length ξ or of the susceptibility χ. For systems belonging to the Ising universality class, a large number of experimental studies could be compared with numerical simulations, with the results of series expansion[2] and with field theoretical models[3]. The dynamics of these fluctuating systems where the microscopic elementary process is the atom spin flip exhibits at the transition a "critical slowing down", corresponding to the divergence of ξ, which is much more difficult to experimentally observe. In a simple diffusion model, the characteristic time τ of the fluctuations should also be divergent at the transition. This model of the dynamics of the transition with "non conserved order parameter", the "A" model of Hohenberg and Halperin[1], see also Ref. 4, introduces a dynamic exponent z, which connects τ to the fluctuations by the following expressions:

$$\begin{cases} \tau(q,T) \propto \xi^z & \text{for } q \ll \xi^{-1} \\ \tau(q,T) \propto q^{-z} & \text{for } q \gg \xi^{-1} \end{cases} \quad (1)$$

where q corresponds to the wavevector. Dynamic renormalization group calculations[5,6,7] as well as Monte Carlo sumulations[8] suggest that $z \simeq 2$.

The order-disorder transformations taking place in the ternary body centred cubic AuAgZn$_2$ alloy have been extensively studied in the 80's in order to determine the thermodynamics and the kinetics associated with the stabilized phases. Close to the critical temperature $T_c \simeq 330°$C, the AuAgZn$_2$ Heussler alloy exhibits a transition between L2$_1$ and B2 structures represented in Fig. 1[9,10]. The transition corresponds to a change of the ordering state in the Au-Ag sublattice leading to a doubling of the unit cell lattice parameter. Above T_c, the two chemical species share a simple cubic lattice. Below T_c, Au and Ag atoms are preferentially located on their own face centred cubic lattices. As the development of or-
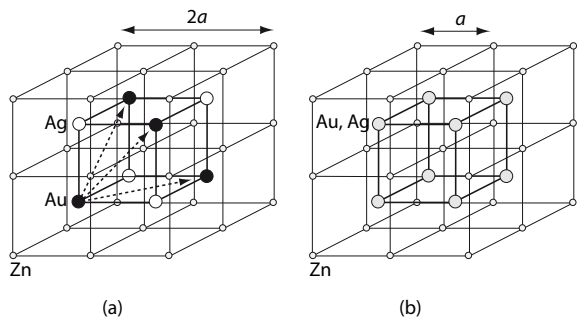

FIG. 1. (a) L2$_1$ and (b) B2 ordered structures of the AuAgZn$_2$ alloy below and above T_c respectively. The lattice parameter a (a_0 in the text) of the B2 phase is close to 3.17 Å at 330°C.

dering does not need a long distance transport of atoms, this alloy can be considered as a model for the transition with "non conserved order parameter", i. e. the "A" model of Hohenberg and Halperin[1].

In a previous paper,[11] the B2→L2$_1$ transition was studied with incoherent X-ray scattering measurements close to the $\frac{1}{2}\frac{1}{2}\frac{1}{2}$ Bragg reflection of the B2 structure. The static critical behaviour was investigated with isothermal acquisitions above T_c to probe the thermodynamical equilibrium. The data analysis has shown a well characterized second-order transition with a transition temperature close to 350°C (varies slightly depending on Zn concentration) and the Ising-like behaviour of the alloy has been confirmed by the values of the critical exponents deduced from the temperature dependence of the intensity profiles. The dynamics of the order-disorder transition was also studied from acquisitions during quenches of the sample. When quench temperatures are well below the critical temperature, the dynamics is mainly associated with the motion of interfaces between ordered domains. The time dependence of the characteristic domains size L was shown to follow the $L(t) \sim t^{\frac{1}{2}}$ growth law, which applies for non-conserved

dynamics far from T_c (see *e.g.* Ref.12). From the equation:

$$L^2 = Dt \qquad (2)$$

the diffusion constant D at the critical temperature was estimated to 2.4×10^5 Å$^2 s^{-1}$ leading to a microscopic diffusion time of $\tau_0 \simeq 40\,\mu s$ between two sites of the Au-Ag simple cubic ($a_0 = 3.2$ Å) sublattice (see Fig. 1b). When quench temperatures are in the vicinity of the critical temperature, the dynamics in a limited time interval is dominated by the time evolution of the critical fluctuations. From the asymptotic behaviour $\xi \simeq a_0(|T - T_c|/T_c)^{-\nu}$, ξ is larger than 500 Å only for $|T - T_c| < 0.2$°C (see Eq. 11 of Ref. 11) and from our estimate of τ_0, the time necessary for their establishment should be roughly 1s with a formula similar to Eq.2, L being replaced by ξ, and writing: $\tau \simeq \tau_0(\xi/a_0)^2 \simeq 40.10^{-6} \times (500/3.2)^2$, in a simple diffusion model (i. e. assuming $z = 2$).

As the elementary process for local ordering is the exchange between neighbouring cubic Au/Ag sites, this system is considered as equivalent to the model "A" of Ref.1.

The experimental observation of the dynamics of the critical fluctuations is a real challenge since heating devices providing high temperature stability, very good accuracy, fast cooling rates as well as small undercooling during quenches are required. A specific water-cooled vacuum chamber with a maximum deviation of 0.01°C for a fixed temperature between 280°C and 365°C and a maximum cooling rate of 2°Cs^{-1} was designed for this purpose and used in our previous study to observe the establishment of the critical fluctuations after quenches. Data analysis in Ref 11 has revealed that 50 s were necessary for fluctuations to have a 500 Å correlation length after quench, which was significantly different from the previous estimate of one second and thus not trustworthy. Further measurements in the AuAgZn$_2$ system at the European Synchrotron Radiation Facility (ESRF) and the Diamond Light Source (DLS) showed us that only the temperature equilibration at long time scales was observed. The reason was found in the poor thermal contact of the ceramic glue with the heating element under vacuum resulting to inertia effects. Because of too slow quenches, the dynamic critical behaviour of the AuAgZn$_2$ ternary alloy could not bee fully characterized in Ref 11 and a reliable comparison with the theoretical predictions is still missing. In the present study, the quality of the thermal contact is improved by inserting a liquid metal drop between the heating element and the samples.

Nowadays, high fluxes of synchrotron sources and high resolutions and counting rates of 2D detectors enable to perform time-resolved diffraction experiments with coherent x-ray beams.[13] This technique called x-ray photon correlation spectroscopy (XPCS) gives rise to new insights into the structure and its dynamics. In coherent scattering experiments, disorder leads to speckles in the measured scattering intensities[13], and the observation of changes in the speckle pattern reflects the microscopic time evolution of the fluctuations.

Pioneering experiments on the dynamics of critical fluctuations have been realized by Brauer *et al*[14] in the Fe$_3$Al binary alloy which exhibits a B2-DO$_3$ second-order transition similar to the B2-L2$_1$ transition investigated in this paper.

In this paper, the x-ray photon correlation spectroscopy technique is used to improve the understanding of the dynamics of critical fluctuations and to determine more reliable estimates of their time correlation functions. Difficulties belonging to this approach are also discussed.

The paper is organised as follows. The first part is devoted to the technical description of the experimental setups, to the characterization of the sample probed by the x-ray beam and to the determination of the degree of coherence of the experiment. In the second part, experimental results are analysed in terms of domain structure, critical temperature assessment and correlation time. The comparison with the theoretical predictions is then presented before concluding remarks.

II. EXPERIMENTAL DETAILS

A. XPCS setup

Most of the results presented here were obtained from dynamic experiments carried out at the Advanced Photon Source (APS), Argonne National Laboratory on the 8ID-G beamline. A few preliminary results were obtained at the I16 beamline of Diamond Light Source (DLS). We used a monochromatic beam of wavelength λ =1.687 Å (APS) and 1.55 Å (DLS) obtained with Si(111) monochromators. At APS, the flux from the undulator was first low-pass filtered by a small mirror 20 m upstream our setup, and at DLS, mirrors were used for vertical focusing and as low pass filters. The transverse beam partial coherence was achieved by slits opened to 20×20 μm upstream the samples. The incident flux at the sample was measured to $\simeq 1.8 \times 10^9$ ph/s at the APS and $\simeq 2.6 \times 10^9$ ph/s at DLS , where pre-focusing optics are used. The scattered intensity was measured with direct illumination CCDs (DI-CCD) from Princeton Instruments. A camera with 1300×1340 active pixels of 20 μm$\times$20 μm size was positioned at 2 meters downstream the sample at APS and a camera with 384×576 pixels of 22 μm$\times$ 22μm size was placed at 2.75 meters at DLS. At the selected wavelengths, the efficiency of the detectors is in the 45-55% range. As these DI-CCDs saturate for about 100 x-rays per pixel, experiments were always carried out with multiple frames, with some dead time between frames. In the case of DLS, the dead time was 0.27 s. In the case of the APS measurements, the dead time between two frames was 1.9 s for full frame (1.7Mpixels at a 1Mhz frequency). For a 1 s exposition
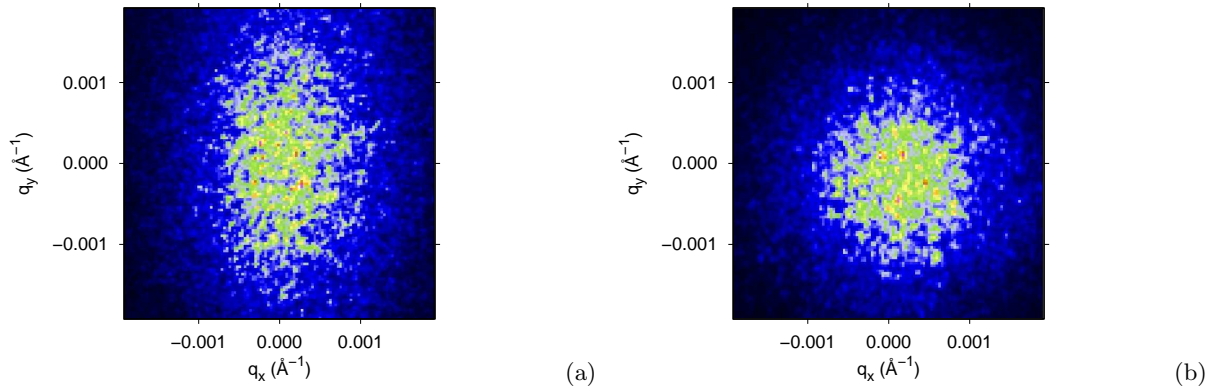
FIG. 2. $\frac{1}{2}\frac{1}{2}\frac{1}{2}$ $(\vec{Q}_0/(2\times\pi))$ Bragg peaks observed at room temperature for (a) a polished sample with an ellipsoidal intensity connected to surface mosaicity (elongation in the q_y direction) and (b) the same sample after disordering and quench showing the isotropic distribution of antiphase boundaries (DLS experiment). $\vec{q} = |\vec{(Q)} - \vec{Q}_0|$ has two components: q_x (nearly parallel to $\vec{Q}_0$) and q_y (perpendicular to $\vec{Q}$)

time, the period of $\simeq 2.9$ s was too slow to observe fluctuation dynamics, and the dynamical measurements were carried out with a 300×300 pixels ROI, which limited the dead time to 0.3 s. The "droplet algorithm"[15] was systematically used for photon counting. If necessary, the x-ray intensity was damped with filters. All the measurements were carried out on the $\frac{1}{2}\frac{1}{2}\frac{1}{2}$ $(=\vec{Q}_0/(2\pi))$ superstructure reflection, which appears owing to the doubling of the unit cell in the ordered phase. In the vicinity of the Bragg position, $\vec{q} = \vec{Q} - \vec{Q}_0$ is the relevant scattering vector. At the critical temperature, the Bragg angle is $\theta_B = 13.32°$ for $\lambda = 1.687$ Å and the x-ray penetration depth in the sample is about 1 μm. The reflection was measured in nearly symmetrical geometry, except for a surface miscut of 2.3° (only for the APS experiment) which was accommodated in the scattering plane. The experimental stability of the setups was confirmed using the static speckle structures from low temperature quenched samples. No significant changes were observed in the structure of the static speckle of the $\frac{1}{2}\frac{1}{2}\frac{1}{2}$ superstructure reflection, which confirmed the good stability in the half hour range at both beamlines.

B. Sample features

Our samples are crystals cut from a single crystal rod 8 mm diameter grown in a vacuum silica ampule, slowly cooled from liquid to $400°C$ and then cooled down to room temperature. This (relatively) fast cooling ($\simeq 2 - 3°C$/s) leads to a pattern of antiphase ordered domains. Samples were then cut with surface normals close to a <111> crystallographic direction, and carefully polished with diamond powder and silica gels.

Experiments carried out at DLS have shown that under vacuum, the surface losses of Zn lead to an inhomogeneous lowering of T_c in the 1 μm depth probed by x-rays. Thus, for the measurements at the APS, a 80 Å

thick aluminum layer has been deposited by sputtering and the resulting Al_2O_3 layer acts as an efficient chemical barrier.

Fig. 2(a) presents a typical scattering map recorded at room temperature for initial microstructures (as-polished samples). The scattering intensity appears ellipsoidal. If samples are then heated above T_c and rapidly cooled down, the enlarged Bragg peak has a circular symmetry as shown in Fig. 2b. In both cases, speckles are observed. The anisotropy observed in Fig. 2a is thus connected to mosaicity caused by the sample polishing yielding scattering elongated along the q_y direction. During this process, a large amount of dislocations are introduced at the sample surface. For temperatures higher than $280°C$, most of this surface dislocation structure disappears and a rapid growth of the $L2_1$ ordered domains is also ob-
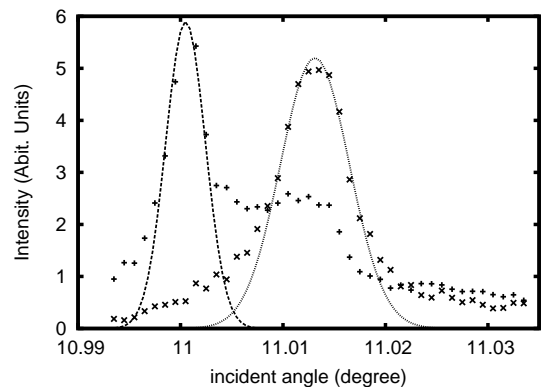

FIG. 3. Rocking curves obtained for two neighbouring positions of the sample (20 μm transverse displacement). Plots from the centers of the peaks show two different values of FWHM: 0.0046° and 0.0079°, and some extra intensity corresponding to defects. The change in the position of the maximum is connected to mosaicity.
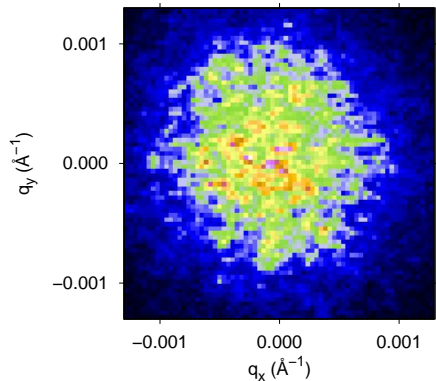
FIG. 4. Typical speckle structure of the $\frac{1}{2}\frac{1}{2}\frac{1}{2}$ reflection (APS experiment) after a rapid cooling down of the sample from disorder to $75°C$C
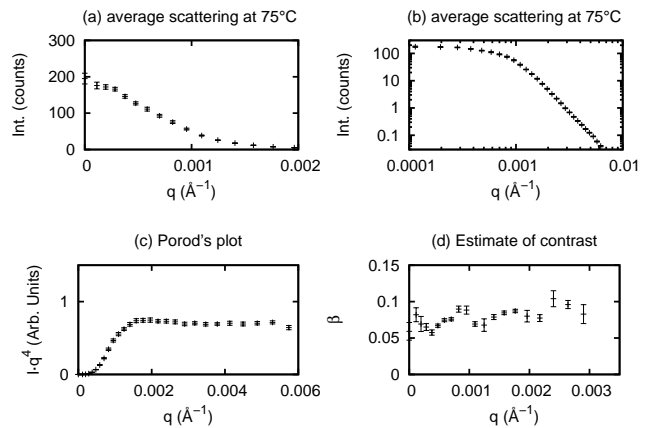

FIG. 5. Circular average of the intensity of Fig. 4. The isotropic intensity corresponds to sets of 50 frames of 1s (a and b). We plot the number of counts per pixel in 50 s (filters were set) and we estimate a domain size of $\simeq 0.15$ μ. "Porod's" plot (c) shows a q^{-4} asymptotic behaviour. This behaviour proves that well defined domains are present, separated by antiphase walls. The speckle contrast β (d) is defined in Eq. 3. We estimate $\beta \simeq 7.5\%$. Our total measurement of 300 frames was split in 6 sets of 50 frames for the estimate of averages and errors.

served. After some aging, a nearly monodomain sample is obtained, but mosaicity can not be entirely removed. This is illustrated for a sample at $336°C$ in Fig. 3 which represents two rocking curves recorded before and after a 20 μm translation of the sample stage. The change in the peak position is connected to some grain structure smaller than the 20 μm beam size. The difference between the peak widths and the intensity profiles show that the microstructure still contains defects. The study of speckles at large angles has to take account of all lattice defects, as it was observed from dislocations[16], or even from surface steps[17]. Experience with metals shows that perfect crystal grains rarely exceed a few micrometers except if annealed for hours close to the melting temperature T_m. In this study, the Zn vapor pressure is too high to carry out a high quality restoration. Consequently, our measurements are sensitive to surface dislocations which move and form subgrain boundaries.

C. Speckle contrast

Coherence can be checked from the isotropic scattering of a quenched sample. Fig. 4 shows the scattering close to $\vec{Q}_0$ observed at APS after a quench to $75°C$. With the hypothesis that no privileged direction in the crystal leads to a systematic anisotropy of the antiphase configuration, the contrast β of our experiment can be estimated from the angular mean square fluctuations of the intensity averaged across rings centered at the Bragg position:

$$\beta(q) = \frac{\langle I(\vec{q})^2 \rangle_{|\vec{q}| \in \Delta} - \langle I(\vec{q}) \rangle^2_{|\vec{q}| \in \Delta} - \langle I(\vec{q}) \rangle_{|\vec{q}|}}{\langle I(\vec{q}) \rangle^2_{|\vec{q}| \in \Delta}} \quad (3)$$

where Δ are domains delimited by circles of increasing radius q: $q - \delta q/2 < |\vec{q}| < q + \delta q/2$. This equation includes a correction for Poisson counting statistics.

The average intensity of Fig. 4 is represented in figures 5a and 5b for two q ranges. The Porod's plot, shown

in Fig. 5c, highlights the q^{-4} asymptotic behaviour of the intensity, thus demonstrating the presence of well defined domains, separated by antiphase walls. The speckle contrast calculated with Eq. 3 is represented in Fig. 5(d) for different values of q. In the case of low (i.e. less than one count par pixel) intensity, the Poisson noise is significantly larger than the speckle contrast. A measurable value of β can nevertheless be obtained, owing to the large number of pixels included in the corresponding domains Δ. By averaging the results between the 6 sets of 50 1s frames, we estimate $\beta = 0.075 \pm 0.01$.

A detailed discussion of the speckle contrast is out of the scope of this paper, but this (relatively) low value is explained by the "large" beam size (20 μm) used, by the poor monochromativity of the beam ($\delta\lambda/\lambda \simeq 0.00014$) with the Si_{111} monochromator, combined with the significant ($\simeq 1$ μm) beam penetration depth. An important contribution to this low contrast is also the asymmetry of the scattering geometry, due to the $2.3°$ miscut of the surface with respect to $\vec{Q}_0$.

III. RESULTS

A. Domain structure

In our samples, scattering in the critical region often exhibits a "two length scale behaviour". This can be observed for example in Fig. 6 where the scattering measured above T_c (at $336.4°C$) is shown. We observe that the "central peak" is slightly anisotropic along $q_z = 0$,
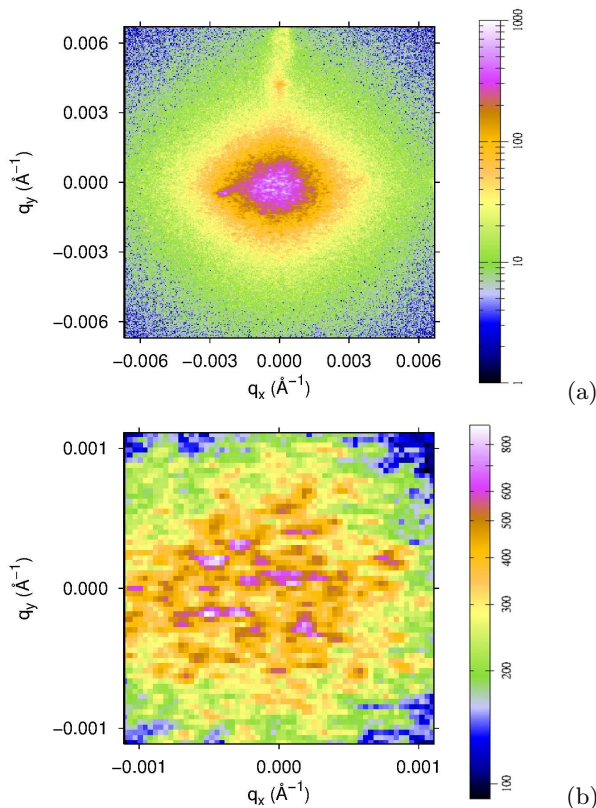
FIG. 6. Scattering observed in the disorder state $(336.4^\circ C \simeq T_c + 0.22^\circ C)$ measured from 200 frames of 1s. Intensities are counts per pixel in 200 s, Measurements were carried out in full frame. (a) shows a large area $(350 \times 350$ pixels) in the center of the detector in logarithmic color scales. The edges of the figure show an isotropic diffuse intensity. Some peaks are observed in the transverse direction (q_y) showing little ordered subgrains with small misorientation (mosaicity) In (b), we observe the details $(50 \times 50$ pixels) of the "central peak" which exhibits a stable speckle structure

probably because it corresponds to a near to surface contribution. We have carried out a circular average of the intensity once a few parasitic peaks observed in Fig. 6 have been discarded, some in the $q_x = 0$ direction corresponding to small misoriented grains and some close to $q_z = 0$ which are observed in Fig. 6. In order to discuss the origin of the intensity of Fig. 6, we fitted this isotropic intensity with the equation:

$$I(|\vec{q}|) = \frac{S(q=0)}{1 + (q\xi)^{1.97}} + \frac{B}{(1 + (qL)^2)^2} \quad (4)$$

The first term $(S(q))$ of Eq.4 gives a rough approximation of the diffuse scattering intensity $(\gamma/\nu = 1.97$ was used[11] which is in fact close to a Lorentzian shape) and the second is devoted to describe the "central peak". A squared Lorentzian was introduced, essentially because of its q^{-4} asymptotic behaviour. Fig. 7 shows the results of the fit when applied to the scattering of Fig. 6. The fit shows the two regimes of the scattering: for $q > 0.003$ Å^{-1}, the fluctuations are dominant, and no speckles are observed.
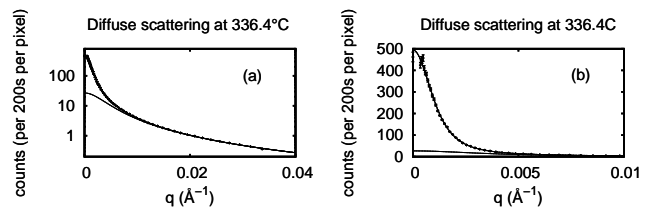

FIG. 7. Angular average of the intensity observed from a 200 s measurement (see Fig. 6) at 336.4°C and a fit with Eq.4: (a) logarithmic plot showing the diffuse scattering, $\xi \simeq 230$ Å and (b) linear plot showing the q^{-4} behaviour of the central peak, $L \simeq 600$ Å
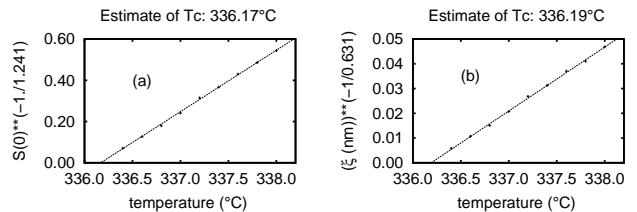

FIG. 8. Results of the fit with Eq.4 for various temperatures. Assuming the Ising static critical exponents, we plot in (a) $S(0)^{-1/\gamma}$ and in (b) $\xi^{-1/\nu}$, $\gamma = 1.241$ and $\nu = 0.631$. Both curves should be linear and should zero out at T_c. We compare our results with fits with Eq. 5) which provide two estimates of T_c $(336.17^\circ C$ and $336.19^\circ C)$. $S(0)$ is in counts per pixel per 200 s and ξ is in nanometers.

For $q < 0.003$ Å^{-1}, the central peak is dominant, it is stable, with visible speckles and its intensity has a q^{-4} behaviour. This means that the pre-transitional peak corresponds to stable limited ordered domains, probably close to the surface.

This "central peak" corresponds to pre-transitional ordering. Moving the sample in the beam modifies its relative weight and shape, but it seems difficult to get rid of it. This behaviour is observed in numerous systems exhibiting second-order transition. It is generally connected to surface defects or surface strain[18],[19].

B. Critical temperature

The "double peak" analysis of Eq.4 provides for each temperature an estimate of S($q = 0$) and of the correlation length ξ. These can be used for the determination of the critical temperature from:

$$S(q=0) = A(T - T_c)^{-\gamma} \quad \text{and} \quad \xi = C(T - T_c)^{-\nu} \quad (5)$$

where the standard static critical exponents in the 3d Ising system $(\gamma = 1.241, \nu = 0.631)$ are used[3],[20]. Fig. 8 shows the results of the fits. We estimate $T_c \simeq 336.18 \pm 0.01^\circ$C.

C. Heterodyne observation of dynamic critical fluctuations

The two components of the scattering in Eq. 4 , as visible in Fig. 6, have different origins: the small ordered domains are essentially stable, leading to observable speckles and the diffuse scattering exhibits no speckles because of short-time fluctuations. The relative weight and shape of the central peak is dependent on the beam position at the sample, but its intensity is strongly temperature dependent.

For the observation of the dynamics, the measuring time was reduced by choosing a 300×300 pixels ROI. Dynamical results were obtained with 0.2 s (0.5 s total period) and 0.8 s acquisition time (i.e. 1.1 s. sampling period).

The standard method is to obtain a doubly-averaged normalized correlation function $g(q,t)$ from the measured intensity $I(\vec{q},t)$:

$$g(q,t) = \frac{\langle\langle I(\vec{q},t+t') \times I(\vec{q},t)\rangle_{t'}\rangle_{|\vec{q}|\in\Delta}}{\langle\langle I(\vec{q},t)\rangle_{t'}^2\rangle_{|\vec{q}|\in\Delta}} \qquad (6)$$

The first average, over the time t' yields a classical time correlation, of poor statistics, and the second average is carried out in the q circular domains Δ, assuming isotropic dynamics.

For short time scales, we observe interference between the stable "central peak" and the fluctuating intensity of the diffuse scattering. This interference has already been observed between a polymer sample and a reference[21], and if one assumes identical coherence factor β for the two scatterer, the speckle dynamics can be written:

$$g(q,t) = 1 + \beta((1-x)^2 + x^2\gamma^2(q,t/\tau) + 2x(1-x)\gamma(q,t/\tau)) \qquad (7)$$

where $x = \langle\langle I_c\rangle\rangle/\langle\langle I\rangle\rangle$ is the mixing, *i.e.* the part of the intensity connected to the critical fluctuations I_c[21]. $\gamma(q,t/\tau)$ is the q-dependent correlation function, which here will be assumed not to differ essentially from an exponential:

$$\gamma(q,t) = \exp(-t/\tau(q)) \qquad (8)$$

In our experiment (see Fig. 6), mixing can be fairly small, and carrying out fits to experimental curves results in x varying from a few percent in the central part to 0.3. This means that the second order term (in x^2) of Eq.7 is nearly negligible.

Typical results are shown in Fig. 9. These data were obtained at $336.25°C$, from 5,000 frames of period 1.1s. Averages were carried out in circles 6 pixels wide, after careful discarding of the mosaic scattering observed in the detector (see Fig. 6). The results of the fits with Eq.7 are shown in the figure. Best estimates of τ were obtained from the measurements displayed in Fig. 9, where $|T - T_c| \simeq 0.07°C$. The results for shorter sampling time or for higher temperatures appear somewhat imprecise. In Fig. 10 are given the results of all fits carried out at
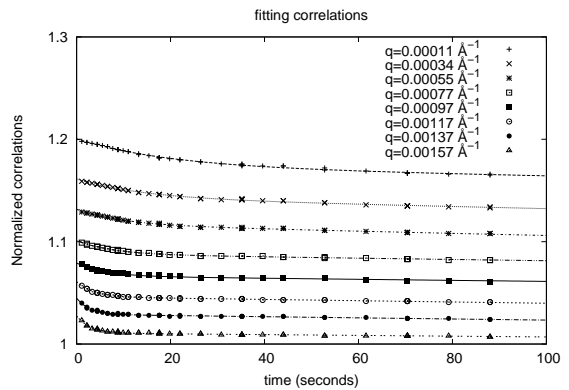

FIG. 9. Time correlations $g(q,t)$ observed at $336.25°$ for various $|q|$ values. Only the results from 5000 frames of 1.1s measured period are shown. Fits correspond to Eq.7. Curves were vertically shifted for better visibility.
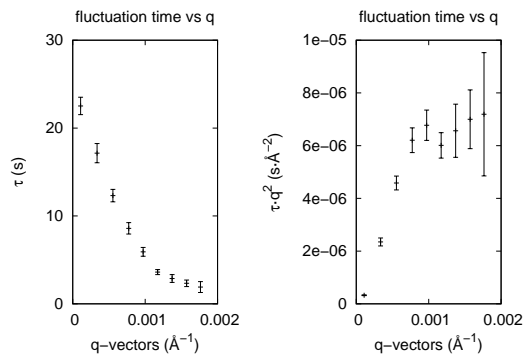

FIG. 10. (left) Estimates of $\tau(q)$ obtained from the set of 5,000 measurements of 1.1 s period and from two smaller sets of 0.5 s period at $336.25°C$. (right) A plot of $q^2 \times \tau(q)$. For this temperature, ξ is of the order of 1000 Å using Eq. 11 in Ref. 11.

$336.25°C$. Results become unreliable for $q > q_{max} \approx 0.002$ Å^{-1}.

In Fig. 10, $q^2 \times \tau(q)$ is also plotted. In the case $z = 2$ is considered valid, this product is constant for $q \gg \xi^{-1}$. From Eq. 11 of Ref. 11, we estimate $\xi \simeq 1000$ Å (for $T - Tc \simeq 0.07°C$), and though q_{max} is not significantly larger than ξ^{-1}, we estimate that this product is close to 7×10^{-6} sÅ^{-2} for large q values. This result can be compared to the observed size increase of the sample after quench. In Fig. 11 is plotted the evolution of the characteristic dimension $\mathcal{L}$ of the domains. In this figure, $\mathcal{L}$ is obtained from the inverse of the half width at half maximum (HWHM) of the scattering observed, different form Eq. 2. In the case of the squared Lorentzian approximation (Eq. 4), $\mathcal{L} = L/\sqrt{\sqrt{2}-1}$. In Fig. 11 a new estimate of the diffusion constant at $334°C$ is given: $D = 4.9 \times 10^5$ Å$^2/s$. This result is consistent with the previous estimate ($D \simeq 2.4 \times 10^5$ Å$^2/s$ (see Eq. 2 in Ref.

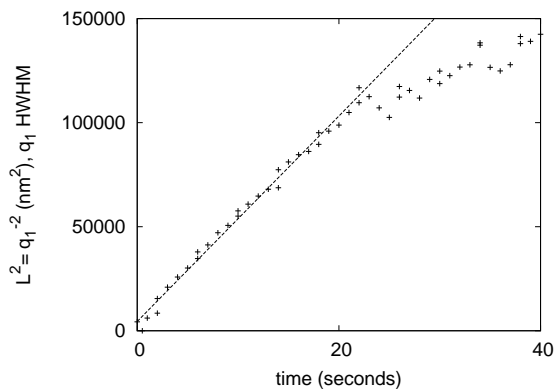FIG. 11. Time evolution of $\mathcal{L} = q_1^{-1}$ at $334.0°C$. q_1 is is obtained from circular averages of the scattered intensity and half width at half maximum estimates. A classical $\mathcal{L}^2 = Dt$ behaviour is observed. The fit corresponds to $D = 4.9 \times 10^5$ $\text{Å}^2/s$.

11), owing to the difference in the definition of domain size.

IV. DISCUSSION

The precise value of z could not be discussed essentially by lack of precision of our results, but also for lack of large variations of fluctuation time and because of the narrow temperature range in the vicinity of T_c where reliable results were obtained. Assuming $z = 2$, the plot of $q^2\tau(q)$ should correspond to the inverse of a diffusion constant. For $q \gg \xi$, this limit seems to be close to 7×10^{-6} sÅ^{-2} (see Fig. 10), and the inverse of this value is 1.4×10^5 $\text{Å}^2/s$ significantly smaller than the diffusion constant ($D = 4.9 \times 10^5$ $\text{Å}^2/s$) as deduced from the ordering kinetics. As we here compare microscopic dynamics (τ_0, the atomic scale diffusion constant) and "mesoscopic dynamics" (the "diffusion" for the hundreds of Angströms scale of the critical fluctuations), a large range of fluctuation lengths are observed. This large range can give an estimate of z. Writing a very rough formula for the dependence of τ on ξ: $\tau \simeq \tau_0(\xi/a_0)^z$, with $\tau_0 = 40$ μs and $\tau = 20s$ for $\xi \simeq 1000$ Å, one obtains $z \simeq 2.28$.

In this paper, we could observe the time dependence of the critical fluctuations for various q vectors and for one temperature in the very vicinity of T_c. In the system studied, the time scale for an atomic jump τ_0 is fairly short ($\simeq 40$ μs), and it is necessary to obtain large scale fluctuations in order to observe their dynamics. A fluctuation length of the order of 300 interatomic distances increases the atomic jump time by a factor $\simeq 10^5$, which gives a fluctuation time in the 1-20 s range. It is $(T - T_c)/T_c \simeq 10^{-4}$, a very narrow temperature domain.

This is to be compared with the dynamic results obtained in the Fe-Al system, where an A2-B2 second order transition of the same universality class (the "A"

model[1]) was also studied for an $Fe_{0.76}Al_{0.24}$ composition. In a "post mortem" study[22], the diffusion constant in the transition vicinity (at about $612°C$) was estimated to 3.2×10^{-17} m^2/s. This means an atomic time scale τ_0 of $\simeq 2 \times 10^{-3}$ s, 50 times slower than in $AuAgZn_2$. This value is in agreement with Ref. 23 where a different definition of the diffusion constant is used. For large fluctuations, the fluctuation time can be in the 100 s range.

This was studied in Ref. 24 by selecting a volume sample of a few μm^3, and by the observation of the scattering at the superstruture Bragg peak position. The results "at T_c" were interpreted as critical fluctuations. The fluctuation time observed "at T_c" was found to be 70 seconds, in agreement with the above estimate. In this paper, the atomic jump time was unrealistically given a value of $\simeq 10^{-7}$ seconds instead of $\simeq 2$ ms, and the authors erroneously claimed a bridge of eight orders of magnitude of time domain.

This is an important remark for future XPCS experiments: when studying large scale dynamics, the microscopic time scale τ_0 which leads the fluctuation dynamics must not be too short, because it it is difficult to observe a slowing down of more than $\simeq 10^5\tau_0$. For instance, in magnetic or in displacive transitions, if the microscopic time scale (spin flip, atom jump) is in the picosecond-nanosecond range, XPCS will not be observable, except with the new x-ray laser sources[25].

The $Fe_{0.76}Al_{0.24}$ alloy gives larger fluctuation times than $AuAgZn_2$ and this should ease the observation of the dynamics of the speckles. Unfortunately, due to x-ray larger penetration depth (several μm) and to lower chemical contrast between ordering elements ($\Delta Z = 13$ for Fe-Al vs $\Delta Z = 32$ for Au-Ag), it may be difficult to carry out dynamic speckle experiments with Fe-Al.

For larger q values ($q > 10^{-3}$ Å^{-1}) and shorter fluctuation times ($\tau < 2s$), improved measurements are now attainable:

1. intensities of the order of 10^{10} coherent photons (for instance ID10 at ESRF, P10 at PETRA III..) are now obtained with improved sources and optics.

2. beam focusing provides beams a few microns wide, opening the opportunity of selecting a smaller sample region (about 10 μm^2 area vs 2000 μm^2 area in this paper) with a smaller number of defects.

3. the new pixel detectors provide a close to unity efficiency and negligible dead time. Their poorer resolution ($\simeq 55\mu m$) is well adapted to smaller beams at the sample in a coherent scattering experiment.

4. in the coming years, many synchrotron facilities will upgrade their storage ring to an achromatic lettice. This should result in an increase a factor $\simeq 30$ of the source brilliance

* frederic.livet@simap.grenoble-inp.fr

[1] P. C. Hohenberg and B. I. Halperin, Rev. Mod. Phys. **49**, 436 (1977).

[2] W. J. Camp and J. P. V. Dyke, Phys. Rev. B **11**, 2579 (1975).

[3] J. C. LeGuillou and J. Zinn-Justin, Physical Review B **21**, 3976 (1980).

[4] R. Folk and G. Moser, J. Phys. A: Math. Gen. **39**, R207 (2006).

[5] C. De Dominicis, E. Brézin, and J. Zinn-Justin, Phys. Rev. B **12**, 4945 (1975), URL http://link.aps.org/doi/10.1103/PhysRevB.12.4945.

[6] A. S. Krinitsyn, V. V. Prudnikov, and P. V. Prudnikov, Theor. Math. Phys. **147**, 561 (2006).

[7] L. Canet and H. Chaté, J. Phys. A: Math. Theor. **40**, 1937 (2007).

[8] P. Grassberger, Physica A **214**, 547 (1995).

[9] M. E. Brooke and R. W. Smith, Scr. Metall. **3**, 667 (1969).

[10] L. Muldawer, J. Appl. Phys. **37**, 2062 (1966).

[11] F. Livet, F. Bley, J. P. Simon, R. Caudron, J. Mainville, M. Sutton, and D. Lebolloc'h, Phys. Rev. **66**, 134108 (2002).

[12] A. J. Bray, Advances in physics **43**, 357 (1994).

[13] M. Sutton, S. G. J. Mochrie, T. Greytak, S. E. Nagler, L. E. Berman, G. E. Held, and G. B. Stephenson, Nature **352**, 608 (1991).

[14] S. Brauer, G. B. Stephenson, M. Sutton, R. Bruning, E. Dufresne, S. G. J. Mochrie, G. Grübel, J. Als-Nielsen, and D. L. Abernathy, Phys. Rev. Lett. **74**, 2010 (1995).

[15] F. Livet, F. Bley, J. Mainville, M. Sutton, S. Mochrie, E. Geissler, G. Dolino, D. Abernathy, and G. Grübel, Nucl. Instr. Meth. **A 451**, 596 (2000).

[16] V. L. R. Jacques, S. Ravy, D. LeBolloch, E. Pinsolle, M. Sauvage-Simkin, and F. Livet, Phys. Rev. Lett. **106**, 065502 (2011).

[17] F. Livet, G. Beutier, M. de Boissieu, S. Ravy, D. L. Bolloc'h, and V. Jacques, Surface Science **605**, 390 (2011).

[18] R. A. Cowley, Physica Scripta **T66**, 24 (1996).

[19] J. Hlinka, R. Currat, M. de Boissieu, F. Livet, and Y. M. Vysochanskii, Phys. Rev. B **71**, 052102 (2005), URL http://link.aps.org/doi/10.1103/PhysRevB.71.052102.

[20] J. C. L. Guillou and J. Zinn-Justin, J. Physique **48**, 19 (1987).

[21] F. Livet, F. Bley, I. Morfin, F. Ehrburger-Dolle, E. Geissler, and M. Sutton, J. Synchrotron Rad. **13**, 453 (2006).

[22] F. Bley, F. Livet, J. C. Leroux, J. P. Simon, D. Abernathy, J. Als-Nielsen, G. Grübel, D. Vignaud, G. Dolino, J. F. Legrand, et al., Acta Cryst. **A51**, 746 (1995).

[23] H. Mehrer, M. Eggersmann, A. Gude, M. Salamon, and B. Sepiol, Mat. Sci. Eng. **A239-240**, 889 (1997).

[24] C. Mocuta, H. Reichert, K. Mecke, H. Dosch, and M. Drakopoulos, Science **308**, 1287 (2005).

[25] G. Gruübel, C. R. Physique **9**, 668 (2008).